Journal of Power Sources 273 (2015) 52–61

Contents lists available at ScienceDirect

Journal of Power Sources

journal homepage: www.elsevier.com/locate/jpowsour

Cycling performance of density modulated multilayer silicon thin film anodes in Li-ion batteries

M.T. Demirkan [a, *], L. Trahey [b], T. Karabacak [a]

[a] Department of Applied Science, University of Arkansas at Little Rock, Little Rock, AR 72204, USA
[b] Chemical Sciences and Engineering Division, Argonne National Laboratory, Argonne, IL 60439, USA

HIGHLIGHTS

- Density modulated Si thin films were investigated for Li-ion battery anodes.
- High/low density Si films were produced by a simple sputter deposition process.
- Alternating low/high Ar gas pressures result in a multilayer high/low density film.
- Superior coulombic efficiency and reversible specific capacity were achieved.
- Density modulated Si films provide enhanced mechanical stability during cycling.

ARTICLE INFO

Article history:
Received 21 July 2014
Received in revised form
28 August 2014
Accepted 3 September 2014
Available online 16 September 2014

Keywords:
Silicon
Thin film
Li-ion
Sputtering
Battery

ABSTRACT

The high volumetric expansion/contraction of silicon (Si) anodes in Li-ion batteries by about ~400% during lithiation/delithiation causes considerably high stress followed by cracking, pulverization, and the loss of electrical contact; and finally results in capacity fading and failing. In this work, we present a new density modulated multilayer Si thin film anode approach, which can provide a robust high capacity electrode for Li-ion batteries. Alternating high and low density layers have been achieved by simply changing the working gas pressure between low and high values, respectively during magnetron sputter deposition of Si thin film anodes. Our results reveal that density modulated Si films can provide a high coulombic efficiency up to 99% and reversible specific capacity as high as ~1700 mAh g^{-1} after 50 cycles. Low-density layers are believed to be performing as compliant layers during volume change making the films more durable compared to conventional Si film anodes. The results of this work can lead to Si thin film anode materials with superior capacity and mechanical stability compared to conventional Si anodes.

1. Introduction

Battery technologies have been gaining substantial importance over the past decade because of the increasing demand for high-power and high-energy density systems especially in electric vehicle and portable electronics applications [1]. Among various types of batteries developed, lithium-ion (Li-ion) batteries can offer superior electrochemical characteristics including high-energy density, high-voltage, and low self-discharge compared to other types of secondary batteries such as nickel–cadmium and nickel-metal-hydride [2]. Because of these unprecedented properties, Li-ion batteries became the most popular battery type in portable electronics such as laptop computers, digital cameras, and cell phones. According to the recent reports [3], annual sales of Li-ion batteries have been steadily increasing, while the others were slowing down over the past few decades.

Intensive investigation is underway on the development of high-capacity cathode materials, yet "high capacity" is theoretically quite limited for intercalation cathodes. High capacity cathode alternatives are limited by the strict chemical criteria for Li-ion batteries [4]. It has become more feasible to increase the capacity of anodes rather than that of cathodes [5]. Therefore, improving the anode capacity is our current topic of focus.

Theoretical properties of some promising Li-ion anode materials are compared in Table 1 [6,7]. Among these materials, significant discoveries have been made in the past decade on the anode

* Corresponding author.
E-mail address: tmdemirkan@ualr.edu (M.T. Demirkan).

http://dx.doi.org/10.1016/j.jpowsour.2014.09.027
0378-7753/

Table 1
Comparison of some of the well-known anode materials for Li-ion batteries.

Charged state of the compound anode	Density of the charged state (g cm^{-3})	Theoretical specific capacity (mAh g^{-1})	Theoretical volumetric capacity (mAh cm^{-3})	Volume expansion (%)
LiC_6	2.02	372	750	10
LiAl	1.35	993	1338	94
Li_3Sb	2.86	660	1888	150
$Li_{22}Sn_5$	2.03	994	2022	259
$Li_{22}Si_5$	0.56	4200	2354	315
$Li_{13}Si_4$	0.62	3103	1939	236

materials such as tin (Sn) and silicon (Si). The exceptionally impressive properties of Si make it very attractive among alternative anode materials; yet, the development of Si anodes has been lagged to produce practical batteries mainly because of the problems summarized below.

Silicon is proposed to be a promising reversible host material for lithium alloying for Li-ion battery anodes [8]. Li–Si alloys can occur in different phases which might have a significant effect on cycling properties of Si anodes. Boukamp et al. [7] showed that each atom of silicon can accommodate 4.4 atoms of lithium in the structure of $Li_{22}Si_5$. A theoretical specific capacity of ~4200 mAh g^{-1} (Table 1) is calculated, which is the highest capacity value among all abundant elements in nature [7]. This makes Si one of the most favorable materials for Li-ion battery anode improvement. Moreover, silicon can be commercially produced at a low cost due to its profusion in nature. The specific capacity of ~3580 mAh g^{-1} for $Li_{15}Si_4$ (cubic) structure was reported with stable cycling, although avoiding this degree of lithiation is advantageous for cycling stability [9,10]. The structure of the $Li_{15}Si_4$ phase is assumed to be the same with $Cu_{15}Si_4$ and $Li_{15}Ge_4$ and was able to hold 2.5 Li ions per Si atom [11]. Change of the silicon structure during Li insertion/extraction generates a significant problem for Li-ion batteries as in some of the metal and metal-oxide anodes (Table 1). Volume change corresponding to a vast expansion of ~236% seem to be the main problem which causes fracturing and pulverization of the Si anode. This mechanical instability leads to poor cycleability and short battery lifetime. In addition, electronic conductivity of Si, which is already low (~10^{-5} S m^{-1}), is further reduced due to pulverization of particles and solid electrolyte interphase (SEI) formation during Li^+ incorporation/removal. Therefore, high volume expansion/contraction of Si during lithiation/delithiation reactions eventually becomes the main reason for degradation of its electrochemical properties. Theoretical and experimental research on the volume expansion of Si is ongoing [12].

Recently, several approaches have been proposed to solve the aforementioned problems with Si anodes. Coatings on Si, using active and inactive additives, Si–C composites, nanostructures of elemental Si and its composites, and Si thin films have been investigated for this purpose [1,5,13]. Using additives or coatings on Si materials were investigated as they can minimize the stress caused by high volume change. They also provide electronical contact between Si particles, which then provides enhanced capacity retention. Among the highest reported capacity values for silicon composite materials, Si powder with carbon nanotube additives showed a specific capacity of 940 mAh g^{-1} [14]. Silicon nanowires are heavily researched as anode materials [15,16], and provided specific capacity values as high as 2800 mAh g^{-1} at the end of 10 cycles [16]. Nano-sized materials can significantly improve the lithium transport properties due to the high surface to volume ratio and high electrode porosity [1]. Nevertheless, the capacity measurements were limited to only a few tens of cycles, which is not sufficient for commercial applications. Recently, CNT-Si core–shell wire composites showed the specific capacity value of ~2900 mAh g^{-1} at the 80th cycle [17]. Another study also reported CNT-Si-Ni nanowires achieving 2000 mAh g^{-1} specific capacity at the 100th cycle [18]. Yi et al. [19] were able to produce Si–C composite materials showing specific capacity value of 1500 mAh g^{-1} at the 200th cycle. Although Si–C composites produced by relatively more well-developed fabrication techniques such as pyrolysis, milling, and chemical vapor reactions have given reasonably good capacity retention (for instance, Kim et al. [20] showed that Si–C composite nanowires can provide a discharge capacity of 2768 mAh g^{-1} with the capacity retention of 87% at the 80th cycle), the requirement of heat treatment, lengthy production times, and in some cases need for nanostructured templates make these methods also significantly complex and expensive [5,21–24]. As another approach, Cui et al. [25] reported a capacity of 1000 mAh g^{-1} and a capacity retention of 90% at the 100th cycle with nanowires that consist of crystalline Si cores and amorphous Si shells. Focus of another study by Yu et al. [26] was to avoid the stress problems using Si ribbons patterned on soft substrates. A capacity retention of 84.6% was achieved at the 500th cycle with a capacity of 3498 mAh g^{-1}. Similarly, Wu et al. [27] proposed the development of Si nanotubes covered with a SiO_x layer to improve the mechanical properties of Si anodes. Capacity values of 1200 mAh g^{-1} at the 600th cycle and 600 mAh g^{-1} at the 6000th cycle were achieved at 1 C and 12 C discharging rates, respectively, for these SiO_x/Si nanotubes. To the best our knowledge, these results seem to be the highest specific capacity values over such large number of cycles ever reported among nanostructured Si anodes. However, fabrication methods of the studies above are often complicated and of high-cost, which make them difficult to be implemented in practical battery applications.

Thin film growth techniques such as sputter deposition or chemical vapor deposition are much more practical and inexpensive compared to the approaches listed above [28]. They are also very well suited for micro-battery and thin film battery applications [29]. In thin film batteries, the components are built layer-by-layer on one another, which is quite compatible with several thin film growth methods [6]. Moreover, thin film anodes have several advantages over bulk materials in Li-ion batteries. They usually provide better stability and capacity retention and they operate kinetically faster due to shorter pathways for Li-ion insertion/deinsertion. Si thin films have proven to demonstrate prominent results with extensively high specific capacities [5,30–34]. However, for practical use of Si thin films in batteries with overall high capacities, they should be thick, at least in micron scales. Growing thicker Si films is a major challenge since it generally suffers from stress build up during deposition followed by delamination from the substrate. Pulverization and stress problems become even worse when the thickness increases. Additional stress during lithiation/delithiation further decrease the mechanical stability. Although it is also a difficult task, improved adhesion of Si to the substrate can partially improve the resistance to stress and

delamination [35,36]. In Table 2, electrochemical properties of Si thin film anodes with thicknesses higher than 400 nm reported in previous studies are summarized. To the best of our knowledge, considering the capacity retention and the capacity values in Table 2, the best performance was reported by Uehara et al. [32] with a 1 μm thick Si thin film anode, which lasted for 200 cycles with a final specific capacity value of 1700 mAh g^{-1}. The high-capacity results in those studies were achieved after additional processing steps such as substrate roughening by chemical etching to enhance film adhesion.

In this study, we report on the development of a density modulated Si thin film approach as the anode material for Li-ion batteries with high capacity and cycling stability. These films consist of Si layers with varying densities and have the ability to tolerate high volume change, stress evolution, and cracking during lithiation/delithiation. This is believed to provide enhanced film stability and better adhesion to the current collector. It was demonstrated that the structural properties of density modulated multilayer thin films by a high/low working gas pressure sputter deposition method provide films with low intrinsic stress, high mechanical stability, and controlled density (porosity) [37,38], which is much desired for battery applications. Multilayer Si thin films proposed in this study are composed of high and low material density layers, where each low density layer acts as compliant that can relax the stress build-up and limits the crack propagation upon volume change during Li insertion/extraction.

Structure and morphology of the films made by sputtering can be controlled depending on several parameters such as temperature, pressure, and voltage. In addition to these, shadowing effect and surface diffusion process are also some important constraints which are described in the well-known "Structural Zone Model (SZM)" [39]. Because of collisions and re-scattering of source atoms as they pass through the working gas (e.g. Ar) and plasma, not all of the atoms come to the substrate directly, and the deposition occurs in a very broad range of angles. At high working gas pressures, atoms go through more collisions due to the denser gas causing lower mean free path values leading to deposition of low density thin films. Therefore, by simply controlling the gas pressure during sputter deposition, one can introduce high and low density films by setting pressure to low and high values, respectively.

2. Experimental

2.1. Fabrication of density modulated silicon thin films

Single and density modulated multilayer silicon thin films were deposited using a multi-source RF/DC magnetron sputtering system (Excel Instruments, India). As illustrated in Fig. 1, the system had two magnetron sputter guns one attached to a DC and the other one to an RF power supply and housing silicon and chromium (Cr) sputter targets, respectively. The substrate modulator, which was at a distance of ~6 inches from the sputter targets, had the

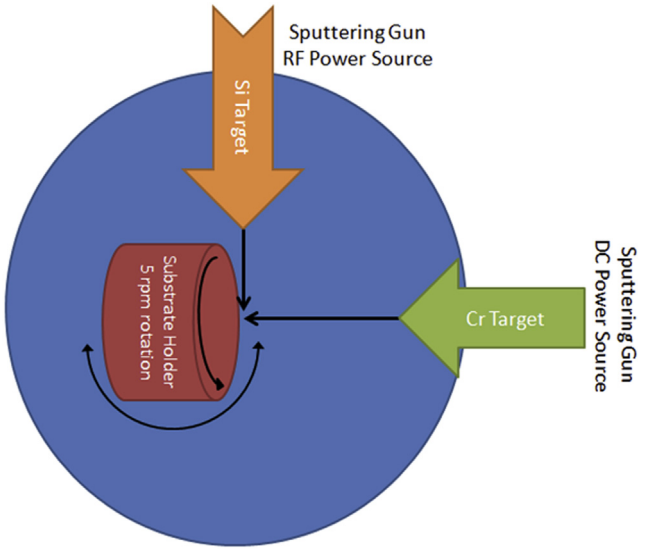

Fig. 1. Illustration of the multi-source sputter deposition system used for the growth of Si thin film anode and Cr adhesion layer. Substrate can be rotated azimuthally around its axis for improved coating uniformity or tilted towards either of the sources for sequential deposition.

substrate tilt and rotation capability controlled by a computer. It allowed tilting the substrate towards the desired sputter guns giving the ability to deposit two different materials after one another. Substrate rotation around the surface normal central axis was utilized to further improve the deposited film thickness uniformity. Circular copper (Cu) foil current collectors were used as substrates for half-cell Li-ion battery tests. Diameter and thickness of Cu foil pieces were 0.5 inches and ~10^{-3} inches (25 micron), respectively. During depositions, quartz crystals (6 MHz, AT cut) and Si wafer pieces (University Wafers, 380 micron, polished) were also included as additional substrates along with Cu foils for the purpose of film density measurements and more convenient cross-sectional scanning electron microscopy (SEM, JEOL – JSM7000F) imaging of the Si thin films, respectively.

A p-type silicon target (Kurt Lesker) with 99.99% purity, diameter of 2 inches, and thickness of 0.125 inch was used as the material source for Si thin films. We used a p-Si target due to the fact that doped silicon films have been shown to provide better electronic conductivity and improved electrochemical performance [31]. A base vacuum pressure of ~3×10^{-6} mbar (~2.3×10^{-6} Torr) was attained using a turbomolecular pump backed by a mechanical pump. An ultra-high purity Ar (99.999% purity, Airgas) was used as the operating gas for generating the plasma. Samples were rotated along the central axis of substrate holder at 5 RPM in order to improve the thickness uniformity of deposited films. Cr target (Kurt Lesker) had a purity of 99.95%, diameter of 2 inches, and thickness

Table 2
Electrochemical properties of a-Si thin film anode materials with thicknesses higher than 400 nm.

Production method	Substrate	Thickness (nm)	Initial charge–discharge capacity (mAh g^{-1})	# of cycles	Last discharge capacity (mAh g^{-1})	Reference
Thermal evaporation	Ni	440	2900–2500	200	1800	Takamura 2004
Thermal evaporation	Ni	520	3000/2500	400	1000	Uehara 2005
Thermal evaporation	Ni	1000	2700/2700	200	1700	Uehara 2005
CVD	Ni	1200	NA/900	20	200	Graetz 2003
CVD	Cu	1200	NA/1000	20	200	Bourderau 1999
Magnetron sputtering	Ni	1200	3300/3000	30	1200	Maranchi 2006
Magnetron sputtering	Cu	1000–2000	3400/2300	30	~1500	Ki-L. Lee 2004
Thermal evaporation	Ni	3600	3100/2300	50	200	Uehara 2005

of 0.12/5 inch. A thin Cr initial layer of about 25 nm thickness was DC-sputter deposited on Cu foils at normal incidence, 150 W power, 2×10^{-3} mbar (1.5×10^{-3} Torr) Ar pressure, and for 2 min in order to improve the adhesion of Si thin films to the Cu substrate. Right after the deposition of Cr adhesion layer, sample holder was turned toward the Si target, and silicon thin films were RF-sputter deposited at normal incidence and at 200 W. This sequential deposition of Cr and Si layers without breaking the vacuum avoids surface oxidation on the Cr/Si interface and provides stronger adhesion and higher electrical conductivity. We did not introduce substrate heating making the process a room-temperature deposition technique.

As described before, thin films with different densities can be produced by controlling working gas pressure values during sputter deposition. Low working gas pressures leads to conventional high density films, while high working pressures cause more porous low density thin films [37,38,40]. Therefore, it is possible to produce density modulated multilayer Si films consisting of low/high material density layers by simply changing the working gas pressure during deposition. In this study, Ar (working gas) pressure value of high density layers was set to 1.5×10^{-3} mbar (1.1×10^{-3} mTorr), while the pressure for low density layers was 1.5×10^{-2} mbar (1.1×10^{-2} mTorr). Ar pressure is controlled by throttling a gate valve between the turbo pump and chamber. Ar flow rate was 10 sccm and kept constant controlled by a flow meter. Deposition rates were measured using the analysis of cross-sectional SEM images, and found to be ~6.1 nm min^{-1} and ~2.8 nm min^{-1} for high density (low Ar pressure) and low density (high Ar pressure) layers, respectively. In this study, we always started with a high-density layer (low Ar pressure) followed by a low density (high Ar pressure) when preparing the density modulated multilayer Si thin film anodes (e.g. Cu/Cr/high-density-Si/low-density-Si/high-density-Si/low-density-Si/for the 4-layer density modulated sample).

2.2. Mass loading measurements

Measuring the weight of thin film and nanostructured coatings can be quite challenging due to their low loading values that typically can range from nanogram to microgram scales. Therefore, small errors in weight measurements of a thin film battery electrode may highly affect the specific capacity value, and for that reason, these measurements should be very sensitive. Some researchers estimated the weight and density of the thin film Si anodes using the theoretical density of Si (2.33 g cm^{-3}) and the thickness values measured from SEM images [30,35,41]. However, theoretical density value can be appropriate only for high density films deposited such as by low-working-gas-pressure sputter deposited thin films. Density of the film can significantly decrease as the working has pressure increases. Therefore, in order to accurately measure the mass loading and calculate the material density of our samples, a quartz crystal microbalance system (QCM) was employed [42]. Frequency values of quartz crystals, which were placed near Cu substrates, were measured before and after the depositions, and mass loadings were calculated using Sauerbrey equation [43].

$$\frac{\Delta m}{A} = \frac{N_q \rho_q}{\pi Z f_L} \tan^{-1}\left[Z \tan\left(\pi \frac{f_U - f_L}{f_U}\right)\right] \quad (1)$$

Equation (1) can be used to calculate the mass of a thin film (i.e. mass change Δm on quartz crystal with units of grams) per unit area using frequency of coated crystal (f_L, Hz), frequency of bare crystal (f_U, Hz), frequency constant for AT-cut quartz crystal (N_q, 1.668×10^{13} Hz Å), piezoelectrically active crystal area (A, cm^2), density of quartz ($\rho_q = 2.648$ g cm^{-3}), Z value (explained below), shear modulus of quartz ($\mu_q = 2.947 \times 10^{11}$ g cm^{-1} s^2), and shear modulus of film (μ_f, g cm^{-1} s^2). Therefore, as the deposition area and the frequencies are known, the weight of the sample can be determined precisely.

Z value is determined as follows:

$$Z = \sqrt{\frac{\rho_q \mu_q}{\rho_f \mu_f}} \quad (2)$$

Film density was then calculated by dividing the measured mass loading to the film volume that was calculated using film thickness values obtained from cross-sectional SEM analysis. QCM method provides a nanograms sensitivity, which allows precise film density measurements.

2.3. Structural characterization and battery tests

Elemental composition analysis was done by energy dispersive X-ray spectroscopy (EDS) attached to the SEM unit. $\theta-2\theta$ scan X-ray diffraction (XRD, Bruker D8) analysis was conducted to study the crystal structure of our Si thin films.

Silicon electrodes deposited on copper foil were cycled in Li-ion coin cells (Hohsen 2032) vs. lithium metal counter electrodes. Cells were assembled in an argon-filled glovebox (<1 ppm O_2 and H_2O) using 1.2 M LiPF6 in 3:7 wt.% ethylene carbonate: ethyl methyl carbonate electrolyte and two Celgard 2325 separators per cell. The coin cells were cycled at room temperature between 10 mV and 1.5 V vs. lithium at 50 μA (40 μA cm^{-2}) on a MACCOR battery tester.

3. Results and discussion

As described above, it is expected that density of conventional Si thin films produced by low-pressure magnetron sputtering should be close to the theoretical density value of bulk Si. In addition, according to SZM, films fabricated at higher working gas pressures should have a columnar structure with lower material density [39]. Therefore, the density of our high-pressure Si thin films is expected to be lower than the theoretical value due to the shadowing effect discussed before. Table 3 summarizes the mass loading and density values of the Cr adhesion layer and Si thin films obtained by QCM weight and cross-sectional SEM thickness measurements. Single layer silicon films deposited at low and high working gas pressures had densities of 2.33 g cm^{-3} and 2.02 g cm^{-3}, which corresponds to 0% and 13% porosity. On the other hand, density modulated multilayer Si films had a density of about 2.22 g cm^{-3} with a porosity value of ~5%, which reflects the average property of high and low density layers. These results agree well with the theoretical predictions of SZM [37,38].

Table 3
Thickness, density, porosity, and weight of the Si thin film samples obtained by quartz crystal microbalance (QCM) weight and cross-sectional scanning electron microscopy (SEM) thickness measurements. Film porosity has been calculated by comparing the measured film density to theoretical density of bulk Si (2.33 g cm^{-3}).

Sample	Film thickness (nm)	Density (g cm^{-3})	Film porosity (%)	Weight (μg)
1-layer low density	74	2.02	13	18.98
1-layer high density	98	2.33	0	28.87
2-layer density modulated	190	2.21[a]	5	53.10
4-layer density modulated	380	2.21	5	106.20
6-layer density modulated	450	2.24	4	127.62

[a] Density of 2-layer sample was calculated using the data from 4-layer sample.

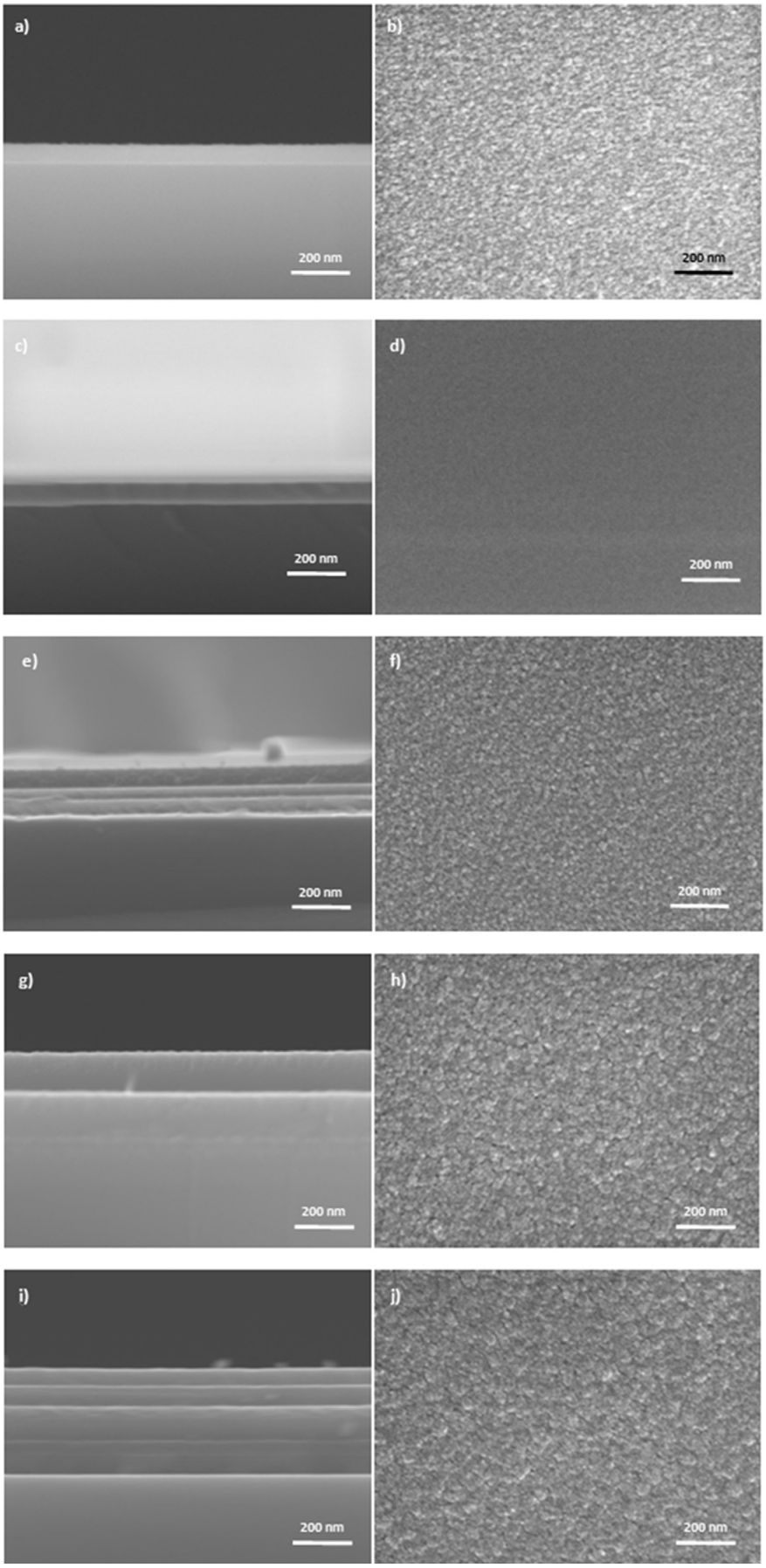

Fig. 2. Cross-section (left column) and top-view (right column) SEM images of a, b) single layer low density, c, d) single layer high density e, f) 2-layer density modulated and g, h) 4-layer density modulated, and i, j) 6-layer density modulated Si thin films deposited on Si substrates.

Cross-sectional and top-view SEM images of the Si thin films on Si wafers are shown in Fig. 2. XRD results (not shown here) did not reveal any peaks indicating all of the films were amorphous. The layers of the density modulated multilayer samples can be distinguished from the cross-sectional images. During the deposition when going from high density to low density, the structure seems to be changing very gradually so it is harder to see the line between high density and low density. The 4-layer sample thus appears to only have 2 layers. However when going from low density to high density, the transition is more drastic so that the line is more visible. During the deposition of the 2-layer sample, there were multiple pauses during the deposition of high-density layer because of the technical issues during deposition. We believe that these pauses caused layers with the same density on top of each other. Therefore the 2-layer sample is seen as if it had more than two layers. As mentioned earlier, more columnar and porous thin films are expected to develop during high-pressure sputter deposition according to SZM. Cross-sectional SEM images (Fig. 2a and c) show that low density layers of Si thin films look more porous compared to the conventional thin films. A rougher surface morphology is also anticipated in low density films due to the high porosity. The porous structure of low density film can be seen on the top-view SEM image (Fig. 2b), which is significantly rougher compared to the high density film (Fig. 2d). As all of our multilayer films ends with low density layers at the top, we can see the rough surface of the low density layer on top-view images of multilayer films (Figs. 2f,j and 3h).

It is well known that adhesion stability of Si thin films on Cu foil is poorer with increased film thickness [11]. Si thin films can be partially or completely delaminated, or cracks can emerge due to the intrinsic stress of thin films [37]. Our preliminary experiments (not shown here) revealed that the delamination occurs with conventional Si films thicker than 150 nm on Cu substrates. In order to achieve better sticking property, a Cr adhesion layer was used in all of our samples sandwiched between the Cu foil substrate and Si films. Although the thickness of our 6-layer sample is almost half of a micrometer, no delamination was observed. This improvement can be attributed to a combination of compliant property of density modulated thin films [37,38] and improved adhesion due to the Cr layer.

Fig. 3 shows the discharge (lithiation) and charge (delithiation) profiles of Si thin film electrodes analyzed for up to 50 cycles. All samples except the 1-layer low density film demonstrated high initial specific capacities approaching ~2500–3500 mAh g^{-1} (charging-discharging). High initial irreversible capacity values are attributed to solid electrolyte interphase (SEI) formation. Samples of 1-layer low density, 1-layer high density, and 6-layer density modulated Si had the poorest capacity retention amongst our samples, having 50th cycle discharge specific capacity values of 185, 222 and 178 mAh g^{-1}, respectively. On the other hand, density modulated Si samples of 2-layer and 4-layer demonstrated much better performance with 50th cycle specific capacities of 1392 and 1704 mAh g^{-1}, respectively, which are higher than most of the silicon anode results reported in the literature (Table 2). We also note that high specific capacity results in previous studies on Si were obtained only after special substrate treatments, unlike the simple, low-cost, environment-friendly, and scalable density modulation process presented in this work. The low cycling performance of the 6-layer sample is believed to originate from higher intrinsic stress of this thicker film that is typically seen in sputter deposited films [38]. This also indicates that thickness of the low density layers that act as compliant need to be optimized, which can further enhance cycling stability for density modulated films and will be the subject of a future study.

A more detailed investigation of the cycling performance and electrochemical properties of the highest capacity sample, the

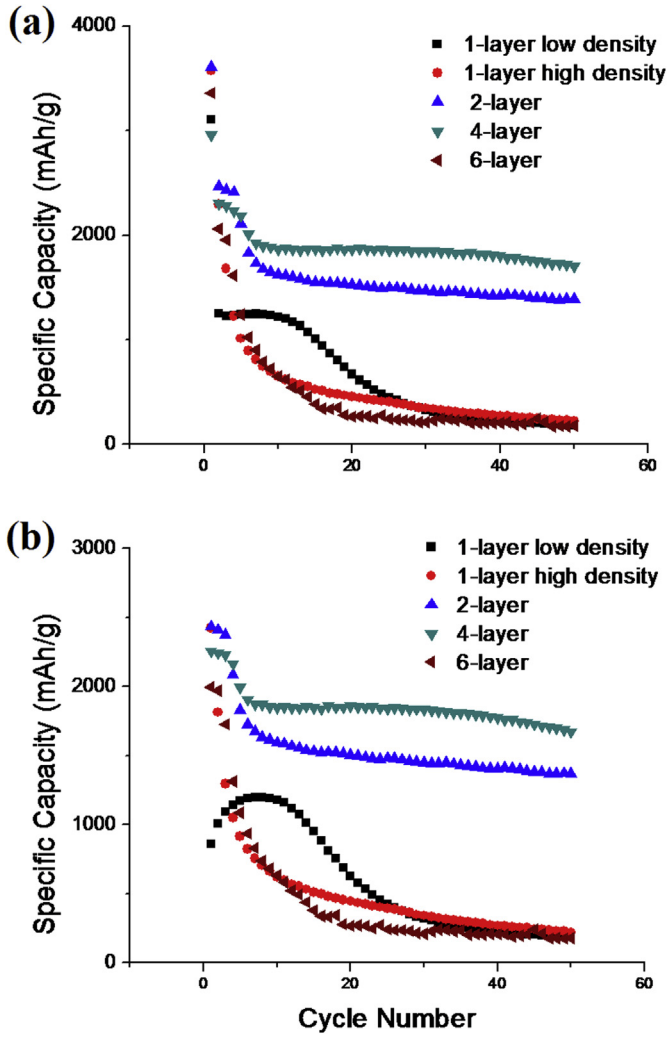

Fig. 3. Discharging (a) and charging (b) profiles of conventional (1-layer samples) and density modulated (2, 4, and 6-layer samples) Si thin anodes.

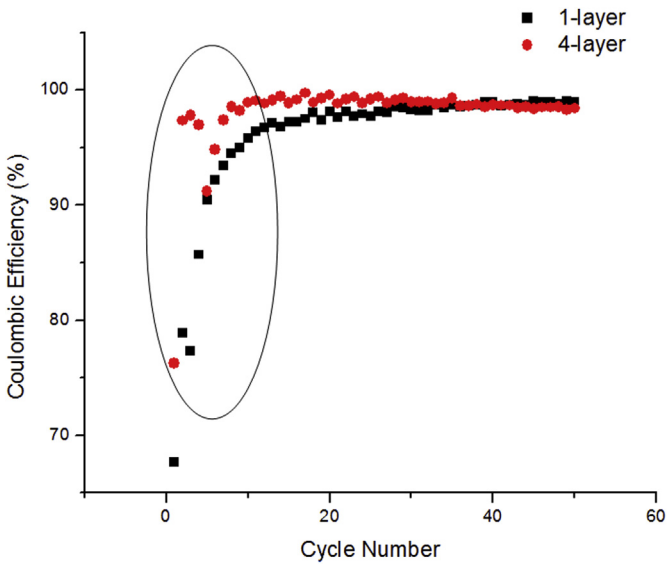

Fig. 4. Coulombic efficiency of single layer high density and 4-layer density modulated Si anodes.

4-layer Si, and the single layer high density Si as comparison is presented in Figs. 4 and 5. Fig. 4 shows the coulombic efficiency over 50 cycles for both samples, with the inset highlighting the first 10 cycles. The best performing sample of 4-layers had a 76% first cycle efficiency, which quickly recovered to >98% after 4 cycles. However, conventional high-density film experienced several low efficiency cycles before stabilizing at >98% after around 30th cycle. Particles coming off the electrode or anode sections not being accessed due to the high density are probable contributors to poor coulombic efficiency. At the end of 50 cycles, the coulombic efficiency of both cells was >98%, which is attributed to good mechanical properties of the 4-layer Si film, and to only a low capacity of material being cycled on the single layer film.

Fig. 5a and b shows the voltage and dQ/dV profiles of select cycles for the conventional single layer high density Si sample. The results are similar to those of the single layer low density and 6-layer samples (not shown). Plateau starting around 0.3 V during lithiation in Fig. 5a is considered to be a characteristic of Li–Si interaction. Fig. 6a and b shows the sample plots for the best electrode tested, the 4-layer density modulated film. Voltage profile and dQ/dV curve of the 4-layer is similar to the results of 2-layer

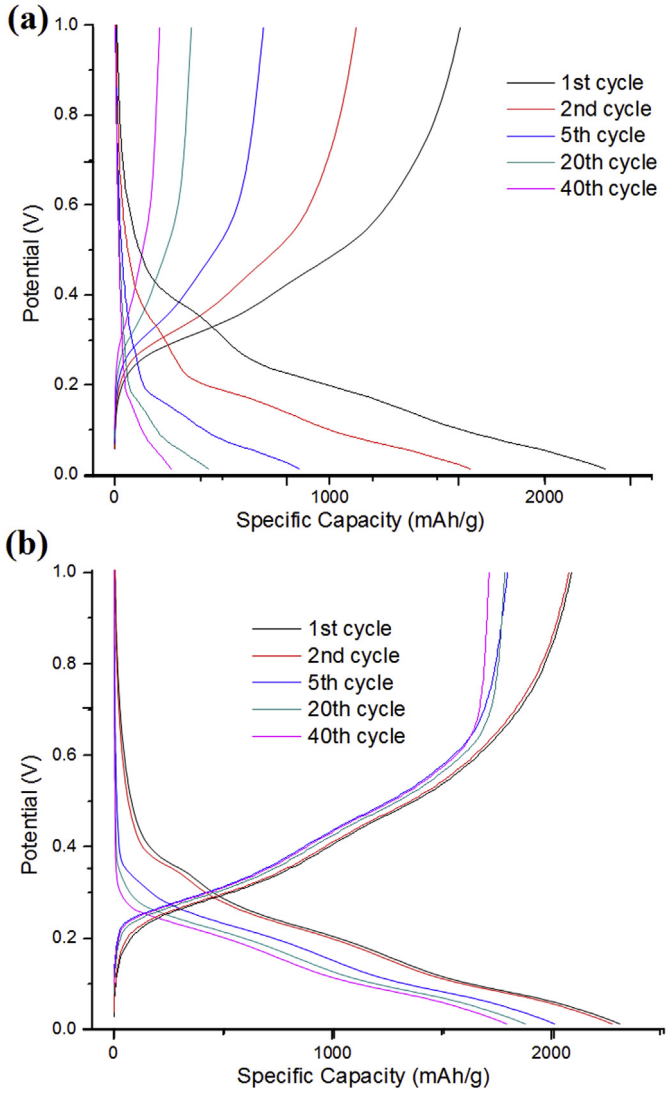

Fig. 5. Voltage profiles of (a) single layer high density and (b) 4-layer samples for first 40 cycles.

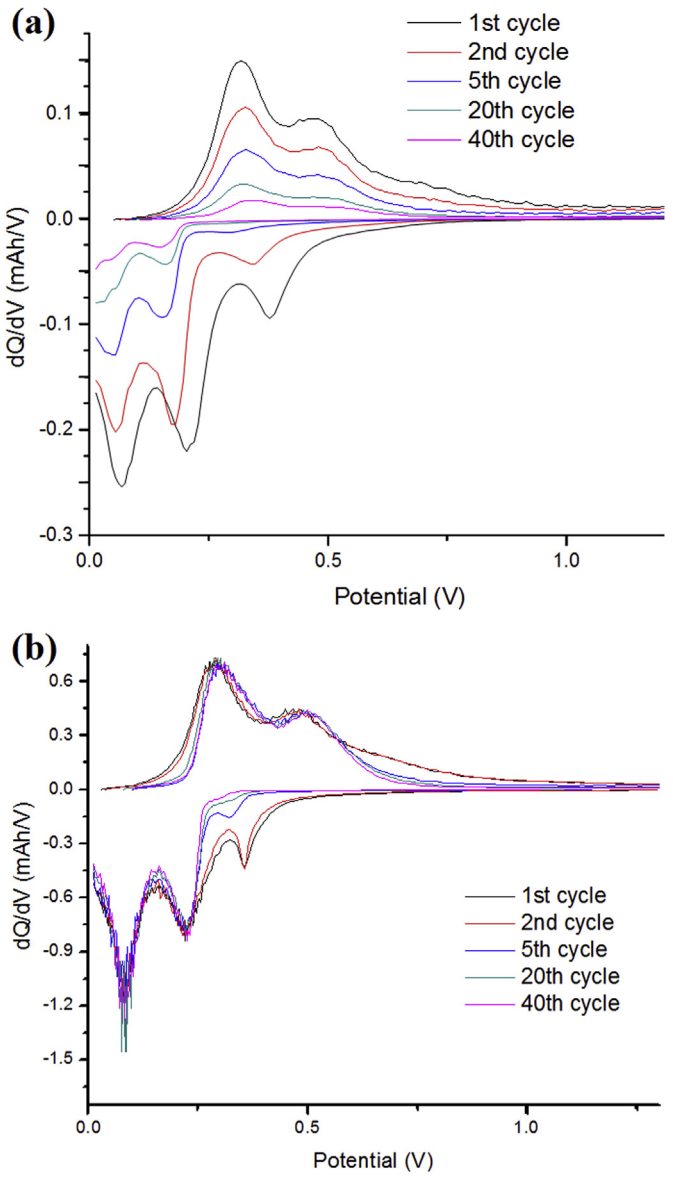

Fig. 6. dQ/dV curves of (a)single layer high density and (b) 4-layer samples for first 40 cycles.

sample (not shown here). In Fig. 6b, the anodic peak at ~0.4 V in the first 2 cycles can be attributed to the SEI layer formation, which later disappears in the 3rd cycle. Anodic peaks at 0.05 V and 0.2 V; and cathodic peaks at ~ 0.3 V and 0.5 V are attributed to lithiation and delithiation of Si, respectively. As the intensity of the peaks decreases in single layer sample in each cycle, amount of reaction lowers down each cycle which indicates the loss of active material during cycling. In contrast, dQ/dV profiles of the 4-layer density modulated Si sample (and similarly also of the 2-layer film) ranging from 3rd cycle up to the 40th cycle overlap perfectly indicating that there is not any notable material loss from the electrode, which further shows the enhanced durability of density modulated Si anodes.

On the other hand, conventional Si thin film anodes reported in previous studies typically show poor stability especially when the film thickness is increased beyond several hundreds of nanometers where stable cycling fails immediately after few tens of cycles [5]. Researchers were able to increase stable critical Si film thickness only after special substrate treatments such as sanding and

chemical etching, which can enhance the contact area and adhesion with the anode film [32], while on the other hand makes the process more complicated, hazardous, and costly. For instance, Si thin films deposited on roughened Cu foils (Table 2, Refs. [44] and [45]) showed specific capacity values of 1200 mAh g^{-1} and 1500 mAh g^{-1} at the 30th cycle. On the other hand, density modulated Si films of this study, which were deposited on untreated current collectors through a much facile process, provided better cycling performance with higher specific capacity values (e.g. the 4-layer density modulated Si anode had a stable ~1700 mAh g^{-1} capacity even after the 50th cycle).

SEM images including EDS weight percentages of Si on the electrodes before and after cycling are shown in Fig. 7 for two of the electrode samples of 4-layer and 6-layer Si, which had high and poor cycling performance, respectively. Single layer and 6-layer thin films were observed to have pulverized/peeled off from the Cu surface after 50 cycles by visual inspection. SEM images and EDS results of Fig. 7a (6-layer sample) shows that these films almost completely came off the Cu current collector and with only some randomly agglomerated particles left over on the surface. EDS analysis show that Si is only found in these particles besides some other residual material from the electrolyte for the 6-layer sample (and similarly for the single layer films; not shown). This indicates that the conventional single layer and 6-layer films mostly delaminated from the substrate, and leftover Si was agglomerated with some residual materials forming cluster-like structures. EDS detects residual materials of F, O and Cr along with Si in those particles while there is only Cu (~%97) and O (~3%) in the empty spaces. On the other hand, according to Fig. 7b, films of 2-layer and 4-layer samples were mostly intact although some limited agglomeration was observed. The SEM micrographs in Fig. 7b show higher resolution images of some of the agglomerated particles. Images show randomly varied arrangement of crack-like separations. EDS results agree with electrochemical cycling results where the 4-layer sample gives the best durability and cycling results amongst our samples.

The main reason for failure of Si as an anode material in Li-ion batteries is the high volume expansion and stress change during lithiation/delithiation as explained earlier. The improvement in the cycling properties of our multilayer Si thin films can be understood in the view of a controlled crack propagation process. When a small crack is initiated in a standard Si thin film, it can move through the whole film until it reaches at the interface where delamination might occur (Fig. 8a). On the other hand, in our density modulated multilayer samples, the borders between each layer can be considered as a grain boundary. Cracking is expected to occur

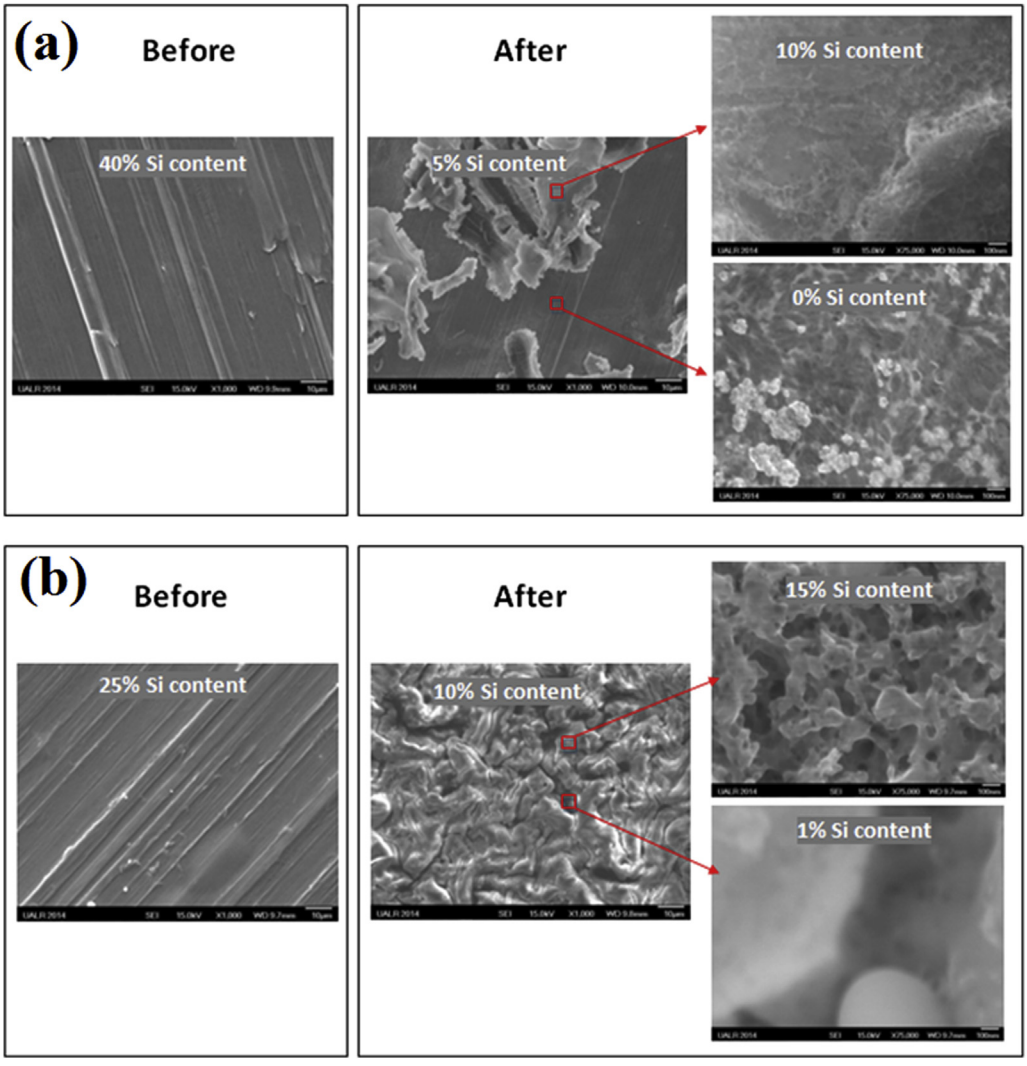

Fig. 7. EDS images of (a) 6-layer and (b) 4-layer samples after electrochemical characterization.

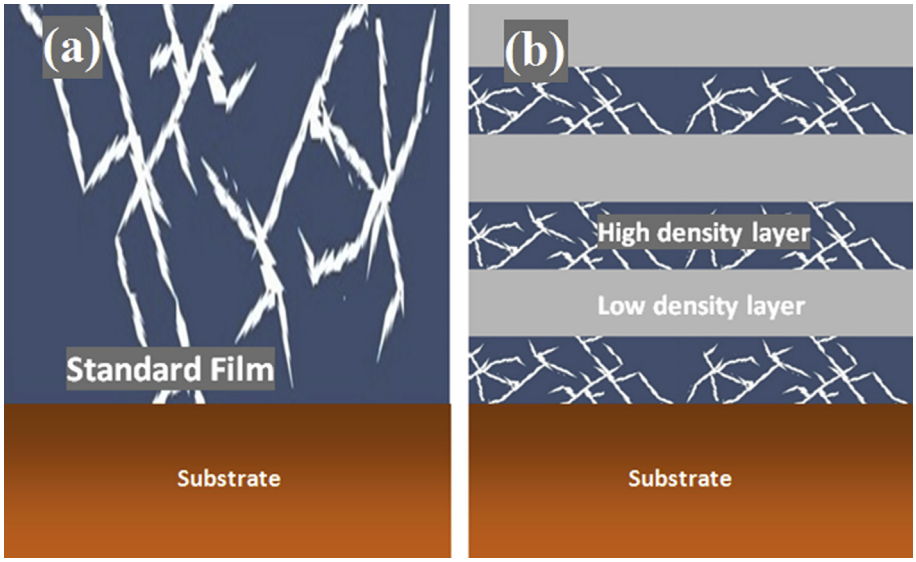

Fig. 8. Demonstration of the crack propagation in (a) standard high density Si thin films and (b) density modulated multilayer Si thin films.

predominantly in high density layers due to their higher volumetric change during lithiation/lithiation, while the low density layers provide a compliant property [46,47] and better accommodate volume expansion/contraction due their higher porosity and surface/volume ratio. Therefore, crack propagation is likely to continue until it stops at the boundary with the neighboring low density layer (Fig. 8b). In other words, density modulation can allow confining the cracks at the high density layers before it causes complete pulverization or delamination of the film, which leads to enhanced toughness of the film. Even if any delamination occurs, it may happen locally or layer by layer thus enhance the stability and the lifetime of the thin film anode.

The high porosity of low density layers can potentially make the diffusion of Li ions into the electrode easier and provides porous pathways for fast Li alloying/de-alloying. On the other hand, denser films are expected to accommodate more Li ions (i.e. due to more Si atoms per film volume) and have better electronic conductivity, yet they are more susceptible to mechanical fragmentation, and lithium diffusion can be more difficult due to the denser structure. Therefore, using high and low density films together can combine their advantageous properties for an optimal Si thin film anode material. It is believed that using a doped Si source to produce electrically more conductive Si films have a notable contribution to the improved properties [32].

4. Conclusion

We report that density modulated multilayer Si thin films incorporating alternating layers of low and high densities produced by a simple high/low pressure sputter deposition process can have the ability to bear the large volume changes and achieve superior cycling stability as anode materials for Li-ion batteries. Electrochemical battery tests done with density modulated Si thin film anodes show that these films can provide enhanced specific capacity and stability properties compared to conventional high density Si films and to those Si films prepared by more complicated, costly, and environmentally hazardous fabrication methods. A 4-layer density modulated sample was still able to hold a reversible capacity of ~1700 mAh g^{-1} at the 50th cycle with a high coulombic efficiency of ~99%. Enhanced cycling performance of density modulated Si anodes is believed to originate from their controlled microstructure which limits the crack propagation and increase the toughness of the film against huge volumetric changes during lithiation/delithiation.

References

[1] F. Cheng, J. Liang, Z. Tao, J. Chen, Adv. Mater. 23 (2011) 1695–1715.
[2] J.M. Tarascon, M. Armand, Nature 414 (2001) 359–367.
[3] Comission, Recommendations on the Transport of Dangerous Goods, United Nations, New York, 2002.
[4] J.B. Goodenough, Y. Kim, Chem. Mater. 22 (2010) 587–603.
[5] U. Kasavajjula, C.S. Wang, A.J. Appleby, J. Power Sources 163 (2007) 1003–1039.
[6] A. Patil, V. Patil, D.W. Shin, J.W. Choi, D.S. Paik, S.J. Yoon, Mater. Res. Bull. 43 (2008) 1913–1942.
[7] G.C.L.B.A. Boukamp, R.A. Huggins, J. Electrochem. Soc. 128 (1981) 4.
[8] R.A. Sharma, R.N. Seefurth, J. Electrochem. Soc. 123 (1976) C239.
[9] Y.H. Xu, G.P. Yin, P.J. Zuo, Electrochim. Acta 54 (2008) 341–345.
[10] M.N. Obrovac, L. Christensen, Electrochem. Solid St. 7 (2004) A93–A96.
[11] T.D. Hatchard, J.R. Dahn, J. Electrochem. Soc. 151 (2004) A838–A842.
[12] S.C. Jung, J.W. Choi, Y.K. Han, Nano Lett. 12 (2012) 5342–5347.
[13] M. Green, E. Fielder, B. Scrosati, M. Wachtler, J.S. Moreno, Electrochem. Solid St. 6 (2003) A75–A79.
[14] J. Shu, H. Li, R. Yang, Y. Shi, X. Huang, Electrochem. Commun. 8 (2006) 51–54.
[15] C.K. Chan, H.L. Peng, G. Liu, K. McIlwrath, X.F. Zhang, R.A. Huggins, Y. Cui, Nat. Nanotechnol. 3 (2008) 31–35.
[16] R. Teki, M.K. Datta, R. Krishnan, T.C. Parker, T.M. Lu, P.N. Kumta, N. Koratkar, Small 5 (2009) 2236–2242.
[17] Y. Fan, Q. Zhang, C.X. Lu, Q.Z. Xiao, X.H. Wang, B.K. Tay, Nanoscale 5 (2013) 1503–1506.
[18] C.X. Lu, Y. Fan, H. Li, Y. Yang, B.K. Tay, E. Teo, Q. Zhang, Carbon 63 (2013) 54–60.
[19] R. Yi, F. Dai, M.L. Gordin, S.R. Chen, D.H. Wang, Adv. Energy Mater. 3 (2013) 295–300.
[20] H. Kim, J. Cho, Nano Lett. 8 (2008) 3688–3691.
[21] A.A. Arie, J.O. Song, J.K. Lee, Mater. Chem. Phys. 113 (2009) 249–254.
[22] C.H. Doh, C.W. Park, H.M. Shin, D.H. Kim, Y.D. Chung, S.I. Moon, B.S. Jin, H.S. Kim, A. Veluchamy, J. Power Sources 179 (2008) 367–370.
[23] Y.R. Ren, M.Z. Qu, Z.L. Yu, Sci. China Ser. B 52 (2009) 2047–2050.
[24] T. Takamura, H. Awano, T. Ura, K. Sumiya, J. Power Sources 68 (1997) 114–119.
[25] L.-F. Cui, R. Ruffo, C.K. Chan, H. Peng, Y. Cui, Nano Lett. 9 (2008) 491–495.
[26] C. Yu, X. Li, T. Ma, J. Rong, R. Zhang, J. Shaffer, Y. An, Q. Liu, B. Wei, H. Jiang, Adv. Energy Mater. 7 (2012) 68–73.
[27] H. Wu, G. Chan, J.W. Choi, I. Ryu, Y. Yao, M.T. McDowell, S.W. Lee, A. Jackson, Y. Yang, L.B. Hu, Y. Cui, Nat. Nanotechnol. 7 (2012) 309–314.
[28] C. Patzig, T. Karabacak, B. Fuhrmann, B. Rauschenbach, J. Appl. Phys. 104 (2008).
[29] N.J. Dudney, B.J. Neudecker, Curr. Opin. Solid St. M 4 (1999) 479–482.
[30] S. Ohara, J. Suzuki, K. Sekine, T. Takamura, J. Power Sources 136 (2004) 303–306.
[31] S. Ohara, J. Suzuki, K. Sekine, T. Takamura, J. Power Sources 119 (2003) 591–596.

[32] M. Uehara, J. Suzuki, K. Tamura, K. Sekine, T. Takamura, J. Power Sources 146 (2005) 441–444.
[33] T. Takamura, M. Uehara, J. Suzuki, K. Sekine, K. Tamura, J. Power Sources 158 (2006) 1401–1404.
[34] J. Yin, M. Wada, K. Yamamoto, Y. Kitano, S. Tanase, T. Sakai, J. Electrochem Soc. 153 (2006) A472–A477.
[35] Y.H. Wang, Y. He, R.J. Xiao, H. Li, K.E. Aifantis, X.J. Huang, J. Power Sources 202 (2012) 236–245.
[36] H. Li, F. Cheng, Z. Zhu, H. Bai, Z. Tao, J. Chen, J. Alloy Compd. 509 (2011) 2919–2923.
[37] T. Karabacak, C.R. Picu, J.J. Senkevich, G.C. Wang, T.M. Lu, J. Appl. Phys. 96 (2004) 5740–5746.
[38] T. Karabacak, J.J. Senkevich, G.C. Wang, T.M. Lu, J. Vac. Sci. Technol. A 23 (2005) 986–990.
[39] J.A. Thornton, Annu. Rev. Mater. Sci. 7 (1977) 239–260.
[40] A. Alagoz, J. Kamminga, S.Y. Grachev, T.-M. Lu, T. Karabacak, 1224-FF05-22, MRS Proc. (2009) 6.
[41] L.B. Chen, J.Y. Xie, H.C. Yu, T.H. Wang, J. Appl. Electrochem 39 (2009) 1157–1162.
[42] M.F. Cansizoglu, T. Karabacak, Paper #: 1216-W05-03, Mat. Res. Soc. Symp. Proc. 1216 (2010).
[43] C. Lu, x Shun, O. Lewis, J. Appl. Phys. 43 (1972) 4385–4390.
[44] J.P. Maranchi, A.F. Hepp, A.G. Evans, N.T. Nuhfer, P.N. Kumta, J. Electrochem. Soc. 153 (2006) A1246–A1253.
[45] K.-L. Lee, J.-Y. Jung, S.-W. Lee, H.-S. Moon, J.-W. Park, J. Power Sources 129 (2004) 270–274.
[46] M.T. Demirkan, X. Li, B. Wei, T. Karabacak, MRS Online Proc. Libr. 1440 (2012) 6.
[47] A.S. Alagoz, J.-D. Kammingaa, S.Y. Gracheva, T.-M. Lua, T. Karabacak, MRS Fall Meeting, vol. 1224, 2009.